Applied Catalysis B: Environmental 132–133 (2013) 13–21

Contents lists available at SciVerse ScienceDirect

Applied Catalysis B: Environmental

journal homepage: www.elsevier.com/locate/apcatb

The effect of carbon nanofiber properties as support for PtRu nanoparticles on the electrooxidation of alcohols

David Sebastián[a], Isabel Suelves[a], Elena Pastor[b], Rafael Moliner[a], María J. Lázaro[a,*]

[a] Instituto de Carboquímica, CSIC, Miguel Luesma Castán 4, 50018, Zaragoza, Spain
[b] Universidad de La Laguna, Dpto de Química-Física, Avda. Astrofísico Francisco Sánchez s/n, 38071 La Laguna, Tenerife, Spain

ARTICLE INFO

Article history:
Received 2 August 2012
Received in revised form 8 November 2012
Accepted 12 November 2012
Available online 24 November 2012

Keywords:
PtRu catalyst
Carbon nanofibers
Fuel cell
Methanol
Ethanol

ABSTRACT

Carbon nanofibers (CNFs) characterized by different mean diameter, BET surface area, pore volume and crystallinity were prepared and studied as supports for PtRu nanoparticles to investigate the influence of the support characteristics on the performance for the electrooxidation of alcohols. A modified microemulsion procedure was used to deposit the metal nanoparticles minimizing the effect of the support on the catalyst particle size.

PtRu nanoparticles of ca. 2 nm size were obtained despite the relatively low surface area of CNFs (95–185 $m^2 g^{-1}$) with a good distribution on the surface as confirmed by TEM micrographs and the high values of the electrochemically active surface areas (110–140 $m^2 g^{-1}$) determined by electrochemical CO stripping. The most appropriate PtRu dispersion was achieved for those carbon nanofibers showing the best compromise in terms of BET surface area and graphicity.

A cross-analysis of the supports physico-chemical properties, ECSA and mass activity for the methanol and ethanol oxidation reactions suggests that both PtRu dispersion and electronic properties as determined by the effect of CNF crystallinity play a significant role in determining the electrocatalytic activity. Different electrocatalytic activity behavior with CNF properties were found for methanol and ethanol. Methanol oxidation is favored using highly crystalline CNFs as PtRu support, despite their low surface area, whereas ethanol oxidation is hindered by diffusional problems when using highly graphitic CNFs due to their low pore volume, so the activity is maximized supporting PtRu on CNFs with a more accessible porosity.

1. Introduction

Energy distribution in low molecular weight alcohols, such as methanol or ethanol, is an attractive option in terms of sustainability and low environmental impact. For their direct conversion into electrical energy, direct alcohol fuel cells (DAFC) are regarded as a very interesting choice in terms of efficiency for portable devices [1–7]. Methanol and ethanol are the most appropriate alcohols in DAFC. Methanol has been widely considered because it is the smallest alcohol molecule and its electrochemical oxidation is relatively fast if compared to alcohols with a higher number of carbon atoms [8]. The use of ethanol instead of methanol has gained interest as it has a higher energy density (about 30% higher), ethanol itself and its oxidation products are less toxic, the cross-over effect is less detrimental and can be easily produced from biomass (a renewable source) [9,10]. Unfortunately, the kinetics of ethanol oxidation reaction (EOR) is even slower than that of methanol oxidation reaction (MOR), where the challenge is the cleavage of C-C bond at low temperature. The improvement of the oxidation kinetics in the DAFC is one of the targets for the implementation of this technology in portable devices, because it would allow increasing the noble metal utilization and reducing the overall cost [7,8]. The current highly performance solid electrolytes based in sulfonated polymers entails the electrooxidation of alcohols in acidic media, which needs the use of expensive noble metallic alloys based on platinum, being the pair platinum-ruthenium widely recognized [11–15].

One of the possible strategies is the optimization of the carbon support. Carbon supports (commonly carbon blacks) are used to maximize the noble metal utilization and reduce costs. The catalyst support is not a mere inert material to disperse the active phase and maximize the metal utilization, but it can also interact electronically with the metal and modify its intrinsic activity [16,17]. During the last decade, carbon nanofibers (CNFs) have been studied as catalytic supports giving place to improved performance in the oxidation of methanol compared to the classical carbon blacks [18,19]. This improved catalytic activity has been attributed to their

* Corresponding author. Tel.: +34 976733977; fax: +34 976733318.
E-mail address: mlazaro@icb.csic.es (M.J. Lázaro).

0926-3373/$ – see front matter © 2012 Elsevier B.V. All rights reserved.
http://dx.doi.org/10.1016/j.apcatb.2012.11.018

good compromise between the external porosity and structural features, derived from the nanosized diameter of the filaments, the orientation of the graphenes with respect to the fiber axis, as well as the high ratio of edge atoms to basal atoms on the surface [20]. Moreover, their peculiar filamentous structure leads to a negligible micropore content, which favors mass transport through the electrocatalytic layers [21]. Additionally, the well-developed graphite-like structure of CNFs can provide a high conductivity and a high resistance to corrosion. The edge-rich surface is expected to provide suitable sites for the stabilization of catalyst nanoparticles. Furthermore, regular arrangement of such sites can provide a more uniform distribution of catalyst particles on the surface [22]. Therefore, the high content of the edge surface is expected to interact with the nanosized metal and to contribute to the stabilization of the nanoparticles on the surface. Investigations up to date regarding PtRu/CNF catalysts include comparing CNFs with carbon blacks [23,24], studying the intrinsic structure in terms of graphene orientation [19,23,25], the study of catalyst properties modifying the metal composition [24], the metal concentration [26], or modifying CNF surface chemistry [27]. Nevertheless, nothing is yet known about the influence of the variation of important properties of CNFs, such as the surface area or the crystallinity, on the performance of PtRu/CNF based electrocatalysts towards the electrooxidation of alcohols.

Carbon nanofibers properties can be adjusted to favor certain processes. In a previous work we observed that a high graphitization degree of functionalized CNFs favors the electrooxidation of methanol on Pt electrocatalysts [20]. In a recent work [28] the effect of support properties has been studied for the reduction of oxygen (cathodic half-reaction) in platinum electrocatalysts, concluding that an optimum activity is found when using carbon nanofibers with a compromise between properties. CNFs also show an enhanced behavior in terms of activity and stabilization of metal particles when compared to the commercial carbon black. Nevertheless, the reaction mechanism is different for every electrocatalytic process and the results regarding the cathodic half-reaction are not extrapolable to the anodic process, as we will demonstrate along this paper. This work is aimed to analyze the effect of different characteristics (diameter, graphitization, etc.) of pristine herringbone type carbon nanofibers on the electrochemical oxidation of methanol and ethanol at low temperature.

2. Experimental details

2.1. Synthesis of PtRu nanoparticles and deposition on carbon nanofibers

In-house synthesized carbon nanofibers with diverse physical properties were used to evaluate their influence on the PtRu catalysts electrochemical behavior. Their synthesis procedure is detailed elsewhere [29,30]. Basically, the carbon nanofiber growth was carried out at five synthesis temperatures between 550 °C and 750 °C (supports will be labeled as 'CNF' followed by the synthesis temperature in Celsius degrees) at low weight hourly space velocity (WHSV) of 4 L g^{-1} h^{-1}, to achieve different graphitization degrees and different porosity features according to previous works [29,30]. Moreover, two additional CNFs were synthesized at higher WHSV (2.5 times higher, 10 L g^{-1} h^{-1}) at 550 °C and 750 °C, labeled as CNF550HV and CNF750HV (HV refers to high velocity). These samples are characterized by a higher pore volume with respect to those obtained at lower space velocity, which will be shown to have an important effect on the catalytic activity. The growth of nanofibers was carried out for enough reaction duration to obtain a high volumetric carbon content of 99%, monitoring the conversion of methane into carbon by gas chromatography. It is known that the synthesis at lower temperatures than 550 °C leads to very low methane conversion, and consequently very low CNF growth rate for practical purposes, whereas synthesis at higher temperatures than 700 °C do not significantly improve crystallinity neither porosity of the nanofilaments, so the selected interval seems to be ideal in terms of the study of the support.

Platinum-ruthenium nanoparticles were synthesized by the water in oil microemulsion route [31,32]. The composition of the microemulsion and the preparation methodology have been adapted and optimized, taking into consideration the peculiar low surface area of carbon nanofibers, in order to obtain high electrochemical surface areas according to previous works with platinum [28]. Briefly, it consists of preparing a microemulsion composed by 16.5% surfactant (polyethylene glycol dodecyl ether, Brij®30, Sigma-Aldrich), 3.9% aqueous solution containing the metal precursors (0.05 M H_2PtCl_6 and 0.05 M $RuCl_3$) and 79.6% n-heptane as the hydrophobic phase. Subsequently, the appropriate amount of carbon support is dispersed in the microemulsion under sonication for at least one hour to achieve a metal concentration in the catalyst of 20 wt.%. The reduction step involves the slow addition of sodium borohydride in excess at room temperature and under vigorous stirring, left overnight under continuous stirring, and finally the catalyst is thoroughly washed with ethanol and water to remove the chemicals used during the synthesis, and dried overnight at 60 °C.

2.2. Solid-state characterization techniques

High-resolution transmission electron microscope (HRTEM) micrographs were obtained using a JEOL-2000 FXII microscope at 200 kV and with a spatial resolution of 0.28 nm. To obtain the micrographs, the catalyst samples were finely grinded and ultrasonically dispersed in ethanol. A drop of the resultant dispersion was deposited and dried onto a standard copper grid coated with Lacey carbon.

The crystallinity of platinum-ruthenium crystallites and carbon was studied by X-Ray Diffraction. XRD patterns were performed using a Bruker AXS D8 Advance diffractometer, using Cu-Kα radiation. Crystallite sizes were calculated from the Scherrer's equation applied to the (002) peak for carbon and (220) peak for platinum related reflections.

Raman spectra were employed to evaluate the ordering degree of CNFs. The spectra were obtained using a Horiba Jobin Yvon HR800 UV, using the green line of an argon laser (λ = 514.53 nm) as excitation source. The carbon ordering degree was evaluated by means of the relative intensities of D (*ca.* 1350 cm^{-1}) and G (*ca.* 1590 cm^{-1}) peaks.

Textural properties of carbon supports such as the specific surface area and the pore volume were calculated from nitrogen adsorption-desorption isotherms, measured at -196 °C using a Micromeritics ASAP 2020. Total surface area and pore volume were determined using the Brunauer-Emmet-Teller (BET) equation and the single point method, respectively. The micropore volume was calculated applying the t-plot method.

Electrical conductivity measurements were also performed pressing the carbonaceous powder at 10 MPa as described elsewhere [30]. The electrical resistance was measured by the four-point probe method applying electrical currents up to 0.02 A.

Energy dispersive X-ray (EDX) analyses and thermogravimetric analyses (TGA) in air were performed to quantify the metal loading in the PtRu/CNF electrocatalysts. EDX measurements were also used to determine the Pt:Ru atomic ratio. An EDX analyzer Röntec XFlash Si(Li) coupled to a Hitachi S-3400 N scanning electron microscope (SEM) was used for that purpose. For TGA experiments in air, a Setaram Setsys Evolution thermogravimetric analyzer was

Table 1
Supports physical-chemical properties.

Support	$D \pm \sigma_D$ (nm)	S_{BET} ($m^2\,g^{-1}$)	ν_{pore} ($cm^3\,g^{-1}$)	Raman I_D/I_G	L_c (nm)	EC_{10MPa} ($S\,cm^{-1}$)
CNF550	24 ± 11	174	0.53	2.39	6.4	2.7
CNF600	28 ± 13	150	0.43	1.87	7.8	3.5
CNF650	46 ± 22	124	0.32	1.53	8.6	4.4
CNF700	54 ± 18	94	0.21	0.87	10.2	13.0
CNF750	63 ± 17	99	0.22	1.03	9.4	17.3
CNF550HV	n.d.	185	0.71	1.76	5.2	1.7
CNF750HV	n.d.	118	0.32	1.42	9.2	10.6

n.d.: not determined

used at atmospheric pressure, and the temperature was varied from room temperature to 950 °C with a constant rate of 5 °C min^{-1}.

2.3. Electrochemical experiments

All the electrochemical experiments were carried out in a half-cell using a three-electrode assembly and an Autolab Potentiostat-Galvanostat. A large area pyrolitic graphite rod served as the counter electrode and a reversible hydrogen electrode (RHE) system was used as the reference electrode. All potentials in the text are referred to the latter. The working electrodes were composed of the electrocatalysts deposited as a thin layer over a pyrolitic graphite disk (7 mm diameter). An aqueous suspension of the catalyst under study was prepared by ultrasonically dispersing it in ultrapure water (Milli-Q) and Nafion. An aliquot of 40 μL of the well-dispersed suspension was pipetted on the top of the pyrolitic carbon disk substrate surface and dried at 80 °C under nitrogen atmosphere, resulting in a metal loading of *ca.* 0.15 mg cm^{-2} (*i.e.* platinum loading of 0.10 mg cm^{-2} for 50 at.% Pt catalysts). After preparation, the electrode was immersed into the deaerated 0.5 M H_2SO_4 electrolyte, prepared from high purity reagents (Merck) and water purified in a Milli-Q system. The electrolyte was saturated with pure N_2 or CO gases (99.997%, Air Liquide), depending on the experiments.

To characterize the PtRu/CNF electrocatalysts, cyclic voltammograms were recorded in the supporting electrolyte solution (0.5 M H_2SO_4) between 0.05 V and 0.85 V vs. RHE at a scan rate of 0.02 V s^{-1}. CO stripping voltammograms were obtained after bubbling this gas in the cell for 10 min at 0.20 V vs. RHE, followed by nitrogen purging to remove the excess of CO. The admission potential was selected considering that for this value maximum adsorbate coverage is achieved for CO adsorption [33,34]. Electrochemical surface active areas were determined from the integration of the CO oxidation region, after correction for double layer capacitance, and assuming 420 μC cm^{-2} involved in the process. Methanol and ethanol electrochemical oxidation reactions were studied by cyclic voltammetry, with a scan rate of 0.02 V s^{-1}, substituting the base electrolyte for a deaerated solution of the corresponding alcohol (2 M) in the base electrolyte (0.5 M H_2SO_4), as described in previous works [20,24]. The stability of the catalysts was evaluated by chronoamperometry at relatively low temperature (*i.e.* for portable devices powered by DAFC), from room temperature to 60 °C, using a jacketed glass cell to which water from a thermostated bath was pumped, at a potential value of 0.5 V vs. RHE (this is, in the activation controlled region).

3. Results and discussion

Physical properties of the CNFs have been varied by means of different synthesis temperatures from 550 °C to 750 °C and two values of weight hourly space velocity, as indicated in the experimental section. Table 1 summarizes the most important properties of the selected CNF samples, including the average nanofiber diameter from TEM images (D), together with its standard deviation (σ_D), the BET specific surface area (S_{BET}), the pore volume (ν_{pore}), the relative intensities ratio between disordered and graphitic Raman peaks (I_D/I_G), the carbon crystal size (L_c) along the c-axis from the broadening of C (002) peak in XRD patterns, and the electrical conductivity of the compressed powder at 10 MPa (EC_{10MPa}).

CNF synthesis temperature influences their properties in two different ways. As a general rule, increasing CNF synthesis temperature leads to the thickening of CNFs, from 24 nm diameter at 550 °C to 63 nm at 750 °C (Table 1), by the effect of catalyst sintering (Ni based). This CNF thickening results in the decrease of the BET specific surface area with temperature, also the decrease of pore volume, but maintaining a negligible percentage of micropores in all cases (*ca.* 1%). Remarkably, BET surface values are found between 94 $m^2\,g^{-1}$ (CNF700) and 185 $m^2\,g^{-1}$ (CNF550HV), which means that even the largest value of surface area is below the typical values found in conventional carbon blacks (*e.g.* 250 $m^2\,g^{-1}$ for Vulcan XC-72R), representing a drawback for the appropriate dispersion of catalytic nanoparticles. On the other hand, the graphitization degree increases with temperature up to 700 °C, both in terms of the Raman I_D/I_G ratio, decreasing from 2.39 to 0.87 with temperature indicating higher ordering degree, and the increase of crystal size (L_c in Table 1), from XRD analyses. A high crystallinity of CNF also favors the electrical conductivity as compiled in Table 1. Moreover, the density of surface defects diminishes with the increase of temperature, as exemplified in the TEM micrographs of Fig. 1. Regarding the variation of space velocity, on the other hand, by comparing CNF550 and CNF750 with CNF550HV and CNF750HV respectively, it leads to a significant change of the pore volume with slight changes in crystallinity. The significant increase of pore volume of 34% for CNF550HV and 45% for CNF750HV but preserving a high crystallinity will result of interest along this paper to evaluate the effect of pore volume on the activity towards the oxidation of alcohols. Notice also that the nanofilament diameter and the surface structure of these two samples (CNF550HV and CNF750HV) is very similar to the corresponding samples obtained at low velocity (CNF550 and CNF750) as evidenced in Fig. 1.

Alloyed PtRu nanoparticles of about 2 nm size and a narrow size distribution are well dispersed on the surface of the seven carbon nanofiber samples, as can be observed in the representative TEM captions of Fig. 1. The increase of both nanofiber diameter and surface ordering degree with synthesis temperature can also be observed in these micrographs, as commented previously.

Table 2 compiles some of the main physical-chemical characteristics of PtRu (1:1 at.) catalysts supported on the different carbon nanofibers. The metal concentration is close to nominal in all cases (20 wt.%), as confirmed by EDX and TGA experiments, with an atomic Pt:Ru ratio of approximately 50:50. The maximum catalytic activity for methanol oxidation has been reported to be given by a broad interval of bulk compositions near 40–60 Pt at.% [11,14,15,35–37]. The effect of Pt:Ru ratio is known to become more important as temperature rises. In this work, the variations of this atomic ratio within catalysts (from 40 Pt at.% in PtRu/CNF550HV to 48 Pt at.% in PtRu/CNF750HV) will be considered enough low to influence the electrochemical behavior (at low

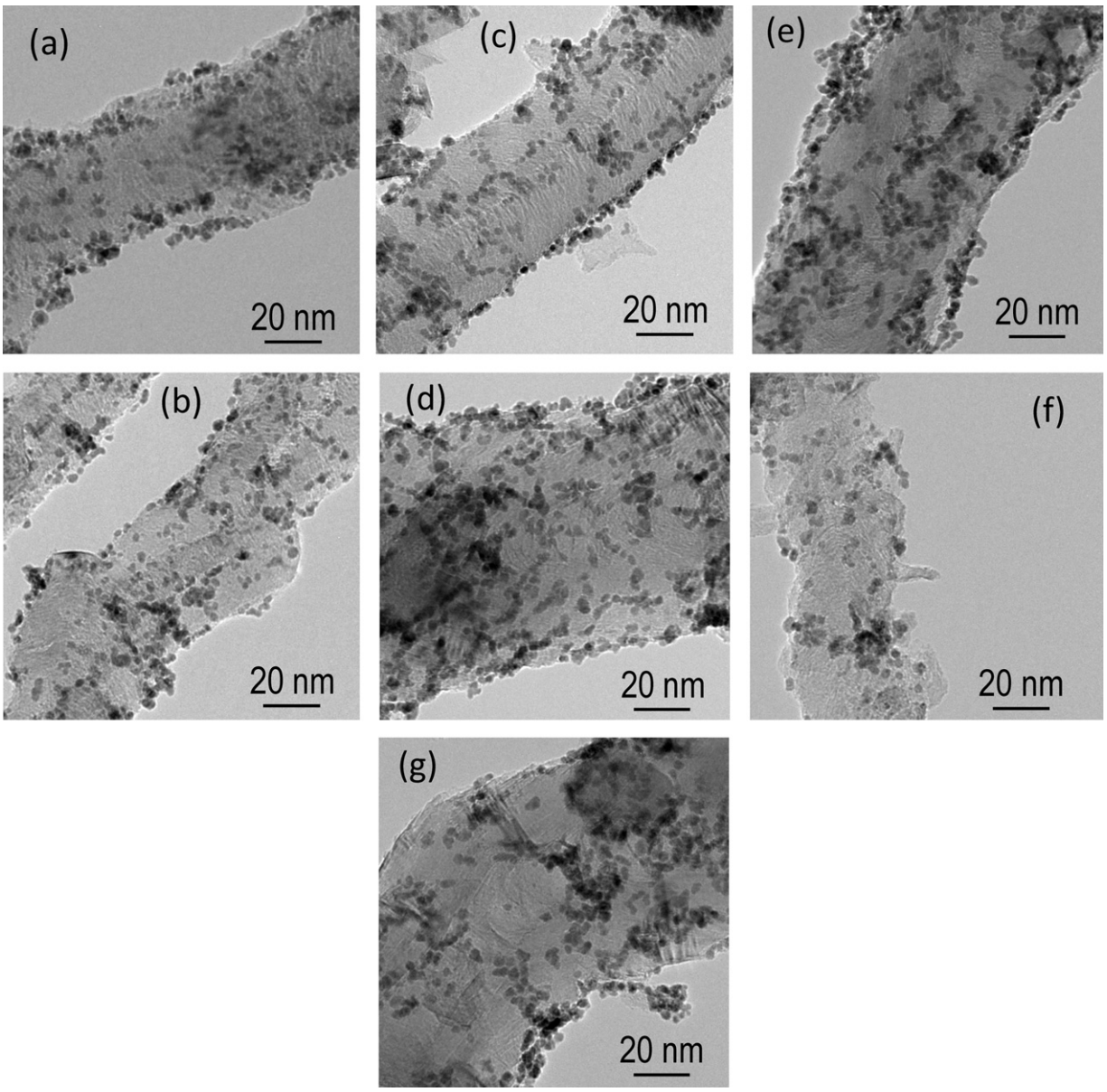

Fig. 1. TEM captions of (a) PtRu/CNF550; (b) PtRu/CNF600; (c) PtRu/CNF650; (d) PtRu/CNF700; (e) PtRu/CNF750; (f) PtRu/CNF550HV; (g) PtRu/CNF750HV.

temperature) in a lesser extent than the variation of CNF properties. X-ray diffractograms (Fig. 2) correspond to the face centered cubic (fcc) structure of platinum, as indicated by the dashed lines, together with the graphitic carbon reflection at *ca.* 26°. The reflections attributed to metal particles are slightly shifted towards wider angles than the corresponding supported Pt, as a result of the alloy with ruthenium. The lattice parameter, calculated from the Bragg equation, is slightly lower than that of pure platinum supported on carbon (*ca.* 0.392 nm) and no reflections associated to Ru, or metal oxides are present, indicating that Ru is alloyed in the platinum structure. PtRu crystal sizes, calculated from the broadening of the (220) reflection and the Scherrer's equation, were found between 1.8 and 2.5 nm. It is to be noted that the average crystal size slightly and progressively increases with the decrease of the CNF surface area, as a result of the slightly higher degree of agglomeration during either the growth or deposition of metal particles, influenced by the surface area of the support. It is also noticeable that the relative intensity of carbon related peak (at *ca.* 26°) with respect to

Table 2
PtRu/CNF electrocatalysts properties.

Sample	PtRu crystal size (nm)	Pt:Ru at. ratio (at.%: at.%)	PtRu concentration (wt.%)	Lattice parameter (nm)	ECSA ($m^2\ g^{-1}$)	TMSA ($m^2\ g^{-1}$)
PtRu/CNF550	1.8	45:55	22	0.388	122	180
PtRu/CNF600	1.9	46:54	18	0.387	142	182
PtRu/CNF650	2.0	43:57	21	0.389	142	160
PtRu/CNF700	2.3	47:53	21	0.388	113	142
PtRu/CNF750	2.7	46:54	22	0.387	104	129
PtRu/CNF550HV	1.9	40:60	19	0.387	63	178
PtRu/CNF750HV	2.5	48:52	22	0.386	101	147

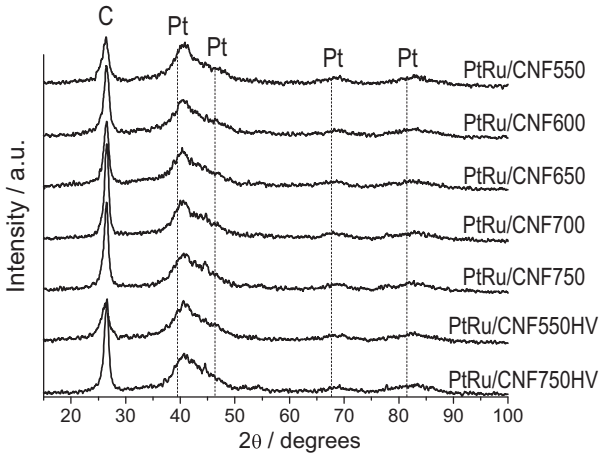

Fig. 2. XRD patterns of 20% PtRu/CNF catalysts.

platinum related peaks increases with the CNF synthesis temperature, as well as the (002) carbon reflection becomes narrower and slightly shifted to higher angles, agreeing to the previous discussion of support graphicity variation with temperature.

Theoretical mass surface areas (TMSAs) were calculated from XRD analyses and according to Aricò and co-workers [15,38]. For this, both the particle size and the degree of alloy were considered to obtain the TMSA assuming spherical nanoparticles and correcting for the value of density. Values were found between 130 $m^2\,g^{-1}$ for PtRu/CNF750 and 180 $m^2\,g^{-1}$ for PtRu/CNF600, significantly high considering the relatively low surface area of CNFs. Previous works regarding low surface area CNFs have reported PtRu crystal sizes that lead to approx. TMSA values of up to 135 $m^2\,g^{-1}$ [24] for a CNF with a S_{BET} of 96 $m^2\,g^{-1}$, whereas other works present lower TMSA values between 60 $m^2\,g^{-1}$ and 120 $m^2\,g^{-1}$ for CNF BET surface areas between 100 $m^2\,g^{-1}$ and 240 $m^2\,g^{-1}$ [23,25,26].

Regarding the electrochemical characterization, Fig. 3 shows the cyclic voltammograms in the oxidation of a CO monolayer, formed at 0.2 V vs. RHE, as well as the second cycle corresponding to the voltammogram of the clean metal surface in the base electrolyte (0.5 M H_2SO_4). The oxidation of CO occurs in a single peak starting at a potential of *ca.* 0.5 V vs. RHE. The peak potential for each sample is indicated in the figure. It is well known that the electrochemical oxidation of CO and alcohols is a surface structure sensitive reaction [1,39,40]. From the CO stripping voltammograms, slight differences (*ca.* 60 mV) are related to the variation of CNF properties, as observed in Pt/CNF electrocatalysts [28], in which the introduction of different CNFs does not considerably change the CO oxidation profile. The minimum differences encountered could be related to the variation of surface structure derived from differences in particle size or to different metal-support interaction in which a higher graphitization degree of the support may favor the electrooxidation of CO at more negative potential values (0.61 V vs. RHE). Nevertheless, these results highlight the fact that PtRu nanoparticles with similar surface structures have been obtained independently of the support features as a consequence of synthesizing metal nanoparticles by means of the microemulsion procedure, which allows the control of metal growth inside micelles. Similar metal surface structures result of key importance for the evaluation of the support properties influence on alcohol oxidation activity.

The electrochemical surface areas (ECSA) were calculated from CO stripping curves assuming a charge of 420 $\mu C\,cm^{-2}$ in the oxidation of a monolayer of linearly adsorbed CO normalized by the total amount of metal (PtRu) [40], and the values are summarized in Table 2. The values of ECSA correspond to highly dispersed PtRu catalysts, in agreement with the low particle size of PtRu

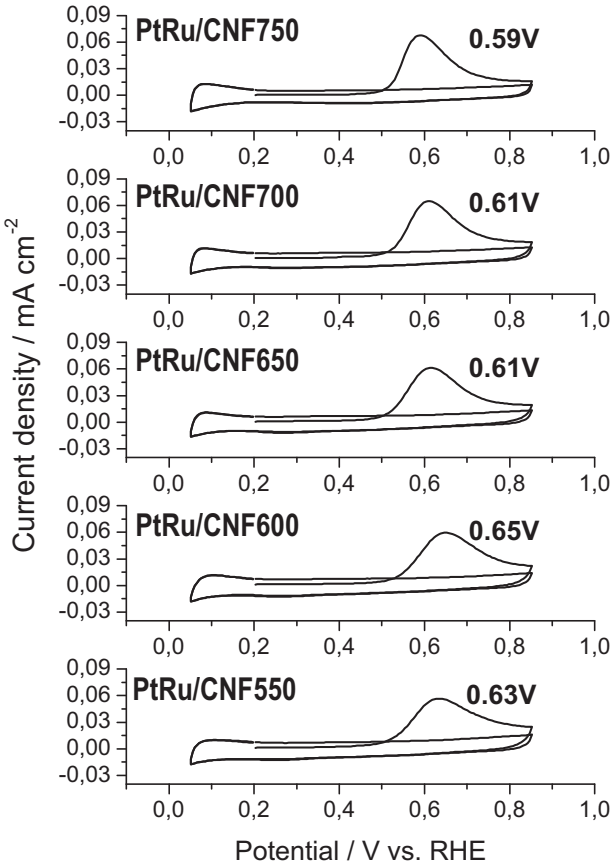

Fig. 3. CO stripping voltammograms at 25 °C and a scan rate of 20 mV s^{-1}, including the CO oxidation peak potential values.

nanoparticles (ca. 2 nm) [41] and their good distribution on the surface as demonstrated in TEM observations. The highest ECSA values, of *ca.* 140 $m^2\,g^{-1}$, are obtained with the catalysts based on CNF600 and CNF650, those supports characterized by their intermediate properties. This can be attributed to their best compromise in terms of support surface area and dispersion as resulting from a moderate concentration of surface groups in the support, in a similar way that observed for platinum catalysts supported on CNFs [28]. Although PtRu particle size was similar among catalysts, significant differences in ECSA were found. On one hand, the variation of particle size in so small nanoparticles leads to significant changes in TMSA values, as indicated in Table 2, from 130 $m^2\,g^{-1}$ to 180 $m^2\,g^{-1}$ corresponding to a variation in PtRu crystal size from 1.8 nm to 2.7 nm. This effect partially explains the variation of ECSA within catalysts. On the other hand, the metal utilization is also influenced by the support surface area. Álvarez and co-workers [42] reported the influence of the ionomer content for two carbon supports with different surface areas (S_{BET}) highlighting the importance of the optimization of the catalytic layer composition to maximize the ECSA. In the present work, the same ionomer concentration has been applied to all catalysts leading to different metal utilization according to their different BET surface areas, and consequently lower than theoretical values. Actually, the ratio ECSA/TMSA is the highest for the catalyst PtRu/CNF650 (89%) decreasing up to approx. 70% for the catalysts with either higher and lower S_{BET}, confirming this hypothesis.

The electrooxidation of methanol (2 M CH_3OH in 0.5 M H_2SO_4) was studied at room temperature by cyclic voltammetry as represented in Fig. 4. An anodic contribution starts at *ca.* 0.4 V vs. RHE, developing an anodic curve which reaches a certain maximum current density value. It is remarkable that the increase

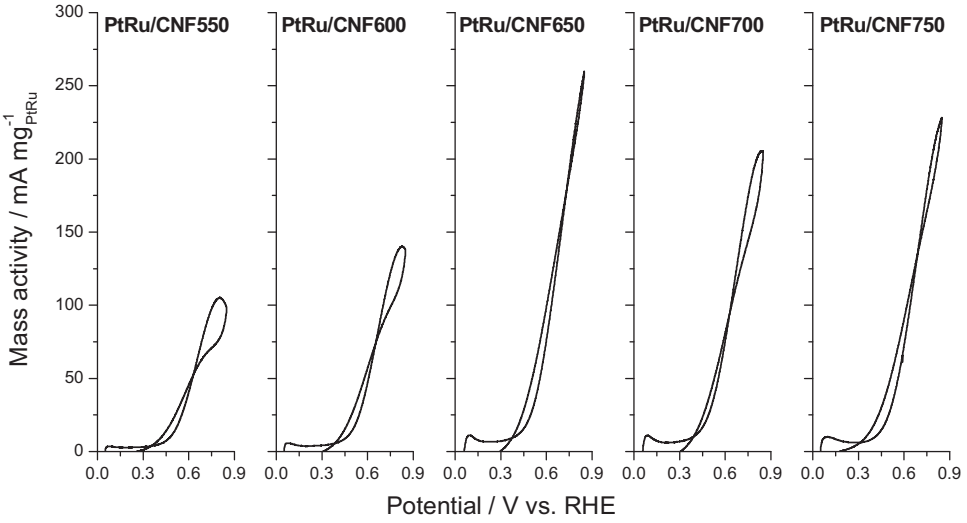

Fig. 4. Cyclic voltammograms for the oxidation of methanol (2 M) in the base electrolyte at room temperature and a scan rate of 20 mV s^{-1}.

of the graphitization degree of the support from CNF550 to CNF650 leads to the increase of this maximum mass activity towards the oxidation of methanol from *ca.* 100 mA mg^{-1} to *ca.* 260 mA mg^{-1}. This rise in activity must be attributed to an enhanced metal-support interaction in highly graphitic carbon nanofibers resulting in the improvement of specific activity, since the differences of electrochemical surface areas (ECSA) do not explain by itself such activity behavior. However, the catalysts based on the CNFs with higher graphicity, (*i.e.* CNF700 and CNF750), present lower maximum activities (*ca.* 205 mA mg^{-1} and 225 mA mg^{-1}, respectively). One must consider separately two contributions to mass activity: the electrochemical surface area (ECSA, $m^2\ g^{-1}$) and the specific or intrinsic activity (the current density per unit of ECSA, μA $cm^{-2}{}_{ECSA}$). This specific activity increases in the order PtRu/CNF550 < PtRu/CNF600 < PtRu/CNF650 ≈ PtRu/CNF700 < PtRu/CNF750, from 85 μA $cm^{-2}{}_{ECSA}$ to 220 μA $cm^{-2}{}_{ECSA}$, this is, as a result of both the increase of particle size (increasing the density of highly active surface catalytic sites) and the enhanced metal-support interaction, due to a higher graphitization of CNFs. However, the ECSA diminishes in CNF700 and CNF750 based samples compared to CNF650 (Table 2), which is not compensated by the increase of intrinsic activity. This results in lower mass activities as represented in Fig. 4. The highest values of mass activity, obtained with PtRu/CNF650 (0.39 mA $\mu g_{Pt}{}^{-1}$) in the cyclic voltammetry, are found in an intermediate region of electrocatalytic activity (between 0.25 mA $\mu g_{Pt}{}^{-1}$ and 1 mA $\mu g_{Pt}{}^{-1}$) according to the review of Brouzgou and co-workers [43]. Even considering that room temperature and lower potential (0.85 V vs. RHE, this is *ca.* 0.65 V vs. Ag/AgCl) were used to evaluate the activity in this work, results are comparable to other novel catalytic structures like core-shell or thin-film Pt based catalysts. This highlights the importance of using highly graphitic mesoporous supports like CNFs to maximize platinum utilization.

A similar approach was carried out to study the electrooxidation of ethanol (2 M CH_3CH_2OH in 0.5 M H_2SO_4). Although it is well known that the catalytic system PtRu is not the optimum for the EOR, being PtSn considerably more active [44–46], the analysis of CNF properties on the behavior of PtRu nanoparticles may be extended to the PtSn system. The corresponding cyclic voltammograms are represented in Fig. 5. It is worth to mention that the current density values obtained in the oxidation of ethanol are comparatively lower than those obtained in the oxidation of methanol (Fig. 4). As discussed in the introduction section, the oxidation of ethanol presents even slower kinetics than the oxidation

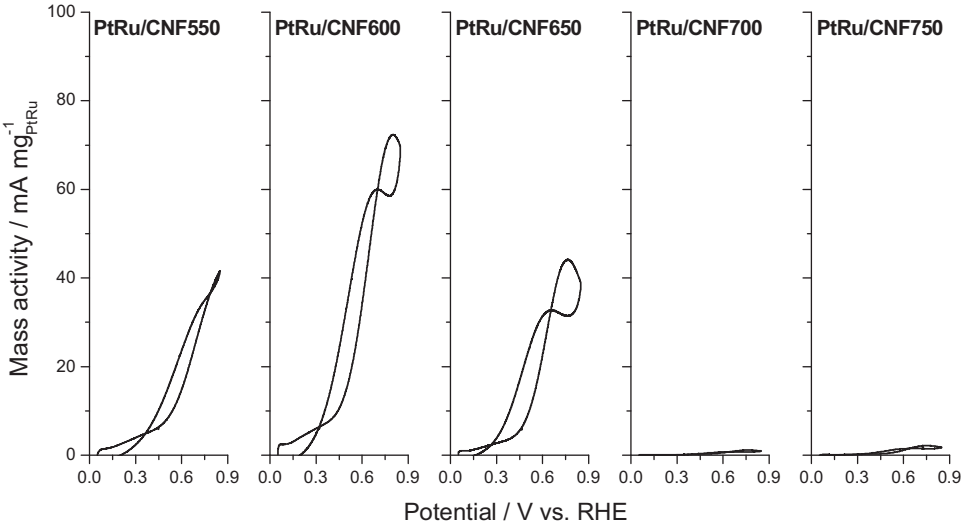

Fig. 5. Cyclic voltammograms for the oxidation of ethanol (2 M) in the base electrolyte at room temperature and a scan rate of 20 mV s^{-1}.

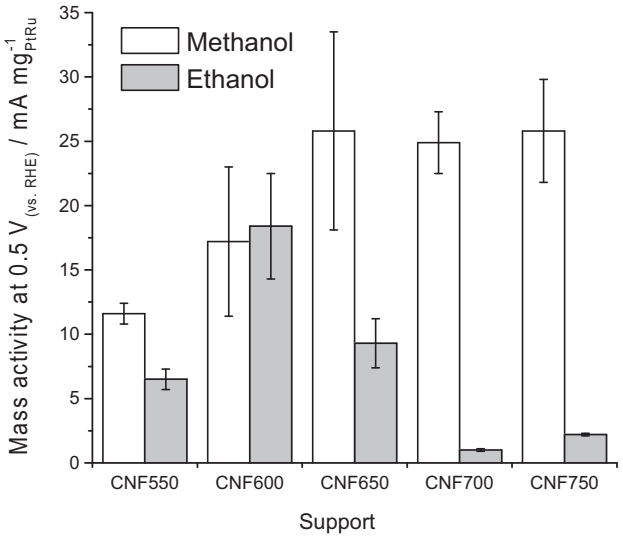

Fig. 6. Comparative chart of the mass activity in the low potential region (0.5 V vs. RHE) for the oxidation of methanol and ethanol according to the CNF used as support for PtRu nanoparticles.

of methanol. The most remarkable result is that the influence of the CNF properties on the activity does not follow the same trend as the observed for the oxidation of methanol. Notice that the best catalysts for MOR, these are, the ones based on highly graphitic supports, give place to considerably lower activity than the best catalyst for EOR, this is PtRu/CNF600. In the case of EOR cyclic voltammetry, the highest mass activity (0.11 mA $\mu g_{Pt}{}^{-1}$) was found again to correspond to an intermediate region of electrocatalytic activity according to the review of Brouzgou and co-workers [43]. However, the decay of EOR activity becomes especially important in the case of PtRu/CNF700 and PtRu/CNF750, which activity is significantly low when compared to the catalysts based on the rest of CNFs. The same trends are found considering the activity at a potential of 0.5 V vs. RHE, this is, in the activation controlled region, as represented in Fig. 6 for the average values of MOR and EOR activity considering the standard deviation from the replication of the experiments. Again, whereas a minimum graphicity is mandatory to maximize the MOR activity with no significant improvement by increasing CNF synthesis temperature beyond 650 °C, the EOR activity presents a maximum value for CNF600.

A plausible explanation of the dramatic decay of EOR activity when using CNF700 or CNF750 may be found when considering their pore volume (0.21 and 0.22 $cm^3\ g^{-1}$ respectively, Table 1). To clarify this phenomenon CNF550HV and CNF750HV, characterized by a higher pore volume than the respective CNF550 and CNF750 (34% and 45% higher respectively), where studied as PtRu support for the electrooxidation of methanol and ethanol. Fig. 7 shows the electroxidation of (a) methanol and (b) ethanol voltammograms for the supports characterized by low pore volume (discontinuous lines) and high pore volume (continuous lines). It is noticeable that the activity towards the oxidation of methanol hardly changes with the use of high pore volume based catalysts, as well as the oxidation of ethanol on CNF550 and CNF550HV based catalysts, but it significantly increases about ten-fold when PtRu is supported on CNF750HV with respect to CNF750. This is a clear indication that the reaction is diffusion controlled when using low pore volume carbon nanofibers in the oxidation of ethanol but this rate determining step changes to kinetic control for high pore volume CNFs.

Stability tests were carried out registering chronoamperometric curves for the electrooxidation of methanol at temperature values between room temperature and 60 °C. Fig. 8 compiles the behavior of two of the catalysts as an example (PtRu/CNF600 and

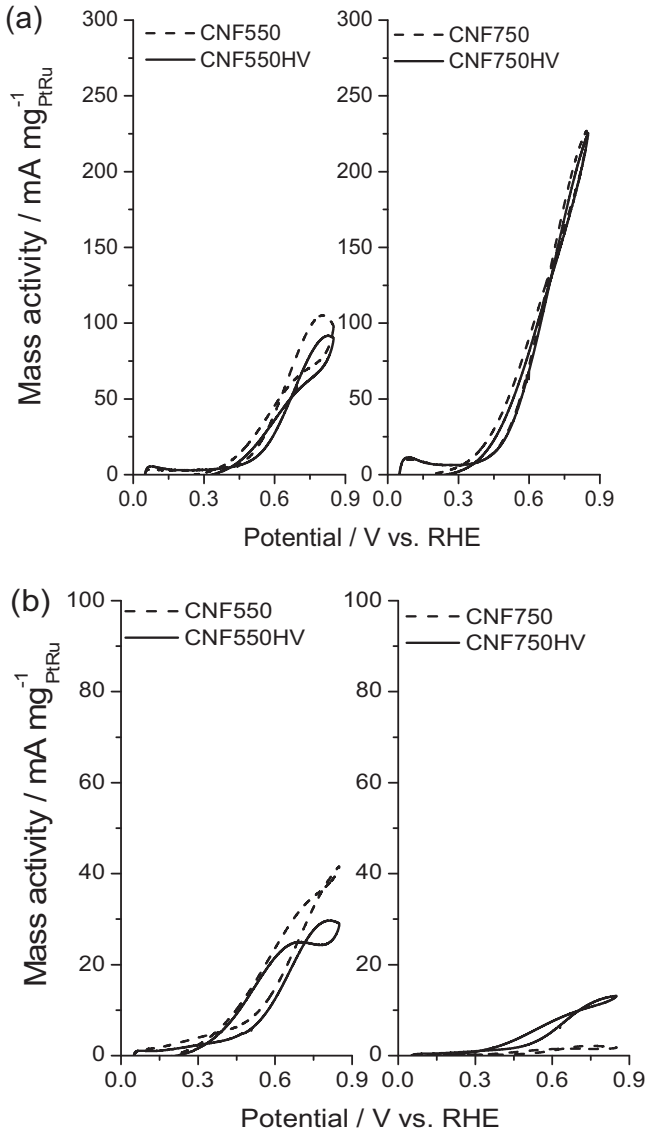

Fig. 7. Effect of the pore volume on the electrocatalytic activity towards de oxidation of (a) methanol and (b) ethanol. The continuous lines (—) represent CNFs with lower pore volume compared to the discontinuous lines (. . .).

PtRu/CNF700) in terms of mass activity at a constant potential (0.5 V vs. RHE), showing all the catalysts the same behavior with activities according to the cyclic voltammograms of Fig. 4. In all cases the stationary current increases with temperature with a slight decrease of performance with time. Activation energy was calculated from the polarization curves obtained at different temperatures (30, 40, 50 and 60 °C), considering the mass activity at 0.5 V vs. RHE and the Arrhenius plot as shown in the inset of Fig. 8(a) and (b). Values in the order of 32–40 kJ mol^{-1} were obtained, very similar among catalysts, this is, no significant effect of support on the activation energy, and comparable to PtRu particles of similar size [38].

To sum up, highly crystalline carbon nanofibers are preferable to obtain a high electrochemical activity towards the oxidation of methanol, independently of fuel cell operation temperature, but a minimum BET surface area is needed to properly disperse nanoparticles and maximize the electrochemical active area and so the metal utilization. In contrast, highly graphitic CNFs are not preferable for the oxidation of ethanol since their worse porous structure hinders the access of such alcohol to the catalytic active sites, concluding that a minimum porosity development is mandatory to

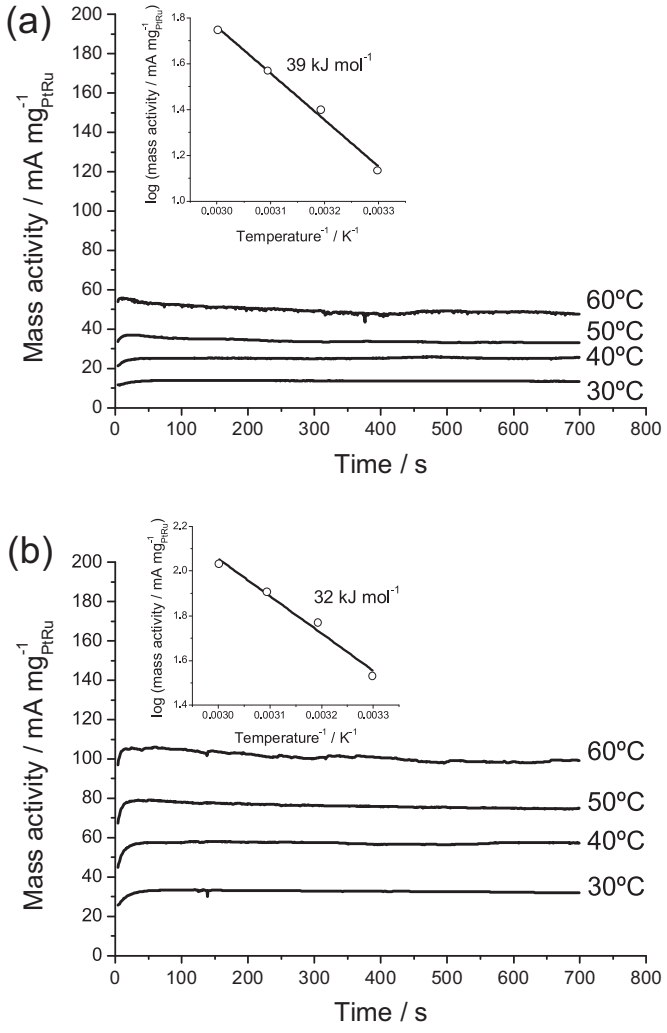

Fig. 8. Stability tests by potential holding at different temperatures and at 0.5 V vs. RHE for the oxidation of methanol (2 M) in the base electrolyte for (a) PtRu/CNF600 and (b) PtRu/CNF700. The inset graphics show the Arrhenius plots for the calculation of activation energy.

obtain a good performance. For the EOR, the pore volume of the support seems to play a very important role.

4. Conclusions

Carbon nanofibers, varying in terms of average diameter, ordering degree, surface structure and porosity, were synthesized and investigated as support for platinum-ruthenium nanoparticles. A microemulsion procedure was employed to synthesize small PtRu nanoparticles of ca. 2 nm with a high electrochemically active surface area and independently of the support features. The catalysts were tested for the anodic electrochemical reaction of direct alcohol fuel cells, analyzing the activity towards the oxidation of both methanol and ethanol. It was observed that the relation between support properties and the electrochemical activity is different for methanol and ethanol oxidation. Methanol oxidation is favored when supporting PtRu nanoparticles on highly graphitic CNFs, being necessary a minimum ordering degree which can be achieved synthesizing the support at 650 °C, despite the worse porous properties compared to the rest of CNFs. On the other hand, the highly graphitic nanofibers that improve the oxidation of ethanol show low activity towards the oxidation of ethanol. Further research has demonstrated that the pore volume may play an important role and consequently CNFs characterized by a more developed porosity maximize the EOR activity despite their lower graphicity.

Acknowledgements

The authors wish to thank FEDER and the Spanish Ministry of Economy and Competitiveness for the financial support to projects CTQ2011-28913-C02-01 and -02.

References

[1] A.S. Aricò, S. Srinivasan, V. Antonucci, Fuel Cells 1 (2001) 133–161.
[2] V. Baglio, A. Stassi, F.V. Matera, V. Antonucci, A.S. Aricò, Electrochimica Acta 54 (2009) 2004–2009.
[3] V. Baglio, A. Stassi, E. Modica, V. Antonucci, A.S. Aricò, P. Caracino, O. Ballabio, M. Colombo, E. Kopnin, Electrochimica Acta 55 (2010) 6022–6027.
[4] C. D'Urso, V. Baglio, V. Antonucci, A.S. Aricò, S. Specchia, U.A. Icardi, G. Saracco, C. Spinella, G. D'Arrigo, International Journal of Hydrogen Energy 36 (2011) 8088–8093.
[5] R. Dillon, S. Srinivasan, A.S. Aricò, V. Antonucci, Journal of Power Sources 127 (2004) 112–126.
[6] S. Song, P. Tsiakaras, Applied Catalysis B 63 (2006) 187–193.
[7] C. Lamy, A. Lima, V. LeRhun, F. Delime, C. Coutanceau, J.M. Léger, Journal of Power Sources 105 (2002) 283–296.
[8] A.S. Aricò, V. Baglio, V. Antonucci, Direct Methanol Fuel Cells, first ed., Nova Science Publishers, New York, 2010.
[9] W. Zhou, Z. Zhou, S. Song, W. Li, G. Sun, P. Tsiakaras, Q. Xin, Applied Catalysis B 46 (2003) 273–285.
[10] P.E. Tsiakaras, Journal of Power Sources 171 (2007) 107–112.
[11] M. Watanabe, M. Uchida, S. Motoo, Journal of Electroanalytical Chemistry 229 (1987) 395–406.
[12] H.A. Gasteiger, N. Marković, P.N. Ross, E.J. Cairns, Journal of Physical Chemistry 97 (1993) 12020–12029.
[13] N. Marković, H.A. Gasteiger, P.N. Ross Jr., X. Jiang, I. Villegas, M.J. Weaver, Electrochimica Acta 40 (1995) 91–98.
[14] O.A. Petrii, Journal of Solid State Electrochemistry 12 (2008) 609–642.
[15] A.S. Aricò, P.L. Antonucci, E. Modica, V. Baglio, H. Kim, V. Antonucci, Electrochimica Acta 47 (2002) 3723–3732.
[16] X. Yu, S. Ye, Journal of Power Sources 172 (2007) 133–144.
[17] E. Antolini, Applied Catalysis B 88 (2009) 1–24.
[18] C.A. Bessel, K. Laubernds, N.M. Rodríguez, R.T.K. Baker, Journal of Physical Chemistry B 105 (2001) 1115–1118.
[19] E.S. Steigerwalt, G.A. Deluga, C.M. Lukehart, Journal of Nanoscience and Nanotechnology 3 (2003) 247–251.
[20] D. Sebastián, J.C. Calderón, J.A. González-Expósito, E. Pastor, M.V. Martínez-Huerta, I. Suelves, R. Moliner, M.J. Lázaro, International Journal of Hydrogen Energy 35 (2010) 9934–9942.
[21] S.-M. Park, D.-H. Jung, S.-K. Kim, S. Lim, D. Peck, W.H. Hong, Electrochimica Acta 54 (2009) 3066–3072.
[22] P. Serp, M. Corrias, P. Kalck, Applied Catalysis A 253 (2003) 337–358.
[23] M. Tsuji, M. Kubokawa, R. Yano, N. Miyaamae, T. Tsuji, s Jun, S. Hong, S. Lim, S.H. Yoon, I. Mochida, Langmuir 23 (2007) 387–390.
[24] N. Tsiouvaras, M.V. Martínez-Huerta, R. Moliner, M.J. Lázaro, J.L. Rodríguez, E. Pastor, M.A. Peña, J.L.G. Fierro, Journal of Power Sources 186 (2009) 299–304.
[25] E.S. Steigerwalt, G.A. deluga, C.M. Lukehart, Journal of Physical Chemistry B 106 (2002) 760–766.
[26] J. Lobato, P. Cañizares, D. Ubeda, F.J. Pinar, M.A. Rodrigo, Applied Catalysis B 106 (2011) 174–180.
[27] J. Guo, G. Sun, Q. Wang, G. Wang, Z. Zhou, S. Tang, L. Jiang, B. Zhou, Q. Xin, Carbon 44 (2006) 152–157.
[28] D. Sebastián, A.G. Ruiz, I. Suelves, R. Moliner, M.J. Lázaro, V. Baglio, A. Stassi, A.S. Aricò, Applied Catalysis B 115-116 (2012) 269–275.
[29] M.J. Lázaro, D. Sebastián, I. Suelves, R. Moliner, J. Nanosci. Nanotechnol. 9 (2009) 4353–4359.
[30] D. Sebastián, I. Suelves, R. Moliner, M.J. Lázaro, Carbon 48 (2010) 4421–4431.
[31] J. Solla-Gullón, F.J. Vidal-Iglesias, V. Montiel, A. Aldaz, Electrochimica Acta 49 (2004) 5079–5088.
[32] S. Eriksson, U. Nylén, S. Rojas, M. Boutonnet, Applied Catalysis A 265 (2004) 207–219.
[33] G. García, J.A. Silva-Chong, O. Guillén-Villafuerte, J.L. Rodríguez, E.R. González, E. Pastor, Catalysis Today 116 (2006) 415–421.
[34] J.C. Calderón, N. Mahata, M.F.R. Pereira, J.L. Figueiredo, V.R. Fernandes, C.M. Rangel, L. Calvillo, M.J. Lázaro, E. Pastor, International Journal of Hydrogen Energy 37 (2012) 7200–7211.
[35] J.B. Goodenough, A. Hamnett, B.J. Kennedy, R. Manoharan, S.A. Weeks, Journal of Electroanalytical Chemistry 240 (1988) 133–145.
[36] Z. Jusys, J. Kaiser, R.J. Behm, Electrochimica Acta 47 (2002) 3693–3706.
[37] T.W. Kim, S.J. Park, L.E. Jones, M.F. Toney, K.W. park, Y.E. Sung, Journal of Physical Chemistry B 109 (2005) 12845–12849.
[38] G. García, V. Baglio, A. Stassi, E. Pastor, V. Antonucci, A.S. Aricò, Journal of Solid State Electrochemistry 11 (2007) 1229–1238.
[39] H.A. Gasteiger, N. Marković, P.N. Ross, E.J. Cairns, Journal of Physical Chemistry 98 (1994) 617–625.

[40] C.L. Green, A. Kucernak, Journal of Physical Chemistry B 106 (2002) 1036–1047.
[41] J.R.C. Salgado, J.C.S. Fernandes, A.M. Botelho do Rego, A.M. Ferraria, R.G. Duarte, M.G.S. Ferreira, Electrochimica Acta 56 (2011) 8509–8518.
[42] G. Álvarez, F. Alcaide, P.L. Cabot, M.J. Lázaro, E. Pastor, J. Solla-Gullón, International Journal of Hydrogen Energy 37 (2012) 393–404.
[43] A. Brouzgou, S.Q. Song, P. Tsiakaras, Applied Catalysis B 127 (2012) 371–388.
[44] W.J. Zhou, B. Zhou, W.Z. Li, Z.H. Zhou, S.Q. Song, G.Q. Sun, Q. Xin, S. Douvartzides, M. Goula, P. Tsiakaras, Journal of Power Sources 126 (2004) 16–22.
[45] W.J. Zhou, S.Q. Song, W.Z. Li, G.Q. Sun, Q. Xin, S. Kontou, K. Poulianitis, P. Tsiakaras, Solid State Ionics 175 (2004) 797–803.
[46] S.Q. Song, W.J. Zhou, Z.H. Zhou, L.H. Jiang, G.Q. Sun, Q. Xin, V. Leontidis, S. Kontou, P. Tsiakaras, International Journal of Hydrogen Energy 30 (2005) 995–1001.